Title: Evaluation of stone features that cause the color Doppler ultrasound twinkling artifact

Author names and affiliations

Eric Rokni[a], Scott Zinck[a], Julianna C. Simon[a]

[a]Graduate Program in Acoustics, The Pennsylvania State University, 201E Applied Science Building, University Park, PA USA 16802

Corresponding author

Eric Rokni

414-379-0684

ezr144@psu.edu

201E Applied Science Building, University Park, PA 16802

Abstract

The color Doppler ultrasound twinkling artifact is a rapid color shift that appears on 43-96% of kidney stones. Surface microbubbles on kidney stones are theorized to cause twinkling as exposure to elevated static pressures of 0.41-1.13 MPa (approximately 0.5-1 times diagnostic ultrasound pressure and 5-10 times ambient pressure), reduced twinkling. However, it is unclear what external and internal stone features support bubbles. Thirteen *ex vivo* kidney stones were scanned with color Doppler ultrasound at 2.5, 5, and 18.5-MHz. Select stones were imaged with environmental scanning electron microscopy (ESEM) or underwater micro-computed tomography (μCT) to evaluate features that may cause twinkling. Results showed the lower frequencies produced larger volumes of twinkling. Condensation first occurred in the smallest (~1 μm diameter) surface pores and may be indicative of where bubbles form. Gas pockets were seen inside 2/3 tested stones that may contribute to twinkling. Overall, these results show evidence of cavity structures both externally and internally and their correlation to the twinkling artifact. This indicates that microbubbles may be present on and within kidney stones and may contribute to the twinkling artifact.

Keywords: kidney stone, Doppler ultrasound, twinkling artifact, microbubbles

Introduction

Kidney stones can form when crystals nucleate in supersaturated urine and interweave with organic matrices composed of proteins and lipids to create a complex heterogenous structure (Khan et al. 2017). This produces a wide range of sizes, structures, and compositions of kidney stones, leading to variable diagnostic success. Computed tomography (CT) is the gold standard to diagnose kidney stones due to its high sensitivity (80-99%), but it also exposes patients to ionizing radiation (Smith & Varanelli 2000). B-mode ultrasound does not expose patients to ionizing radiation but has a wide variation in sensitivities (19%–93%), as accurate detection of stones is highly dependent on the skills of the operator (Sorensen et al. 2013). The color Doppler ultrasound "twinkling artifact" is a rapid color change that highlights 43-96% of kidney stones (Aytaç and Özcan 1999; Dillman et al. 2011; Kielar et al. 2012; Korkmaz et al. 2014; Lee et al. 2001; Masch et al. 2016; Park et al. 2008; Turrin et al. 2007; Winkel et al. 2012; Wood et al. 2020) and can help differentiate kidney stones from the surrounding tissue. Although the twinkling artifact has been shown to be a useful diagnostic tool for kidney stones, it is yet unclear why not all stones twinkle (Lee et al. 2001; Trillaud et al. 2001; Mitterberger et al. 2009; Shabana et al. 2009). The goal of this paper is to determine what physical features of the stone contribute to the color Doppler ultrasound twinkling artifact.

Two hypotheses have been used to describe the origin of the twinkling artifact: ultrasound phase jitter/machine settings and the interaction of the acoustic wave with the stone. Phase jitter has been proposed to produce twinkling through perceived Doppler shifts caused by slight fluctuations in the time synchronization of ultrasound machines that could be accentuated by rough surfaces (Kamaya et al. 2003). However, more recent research has shown

phase jitter is not a significant contributor to twinkling (Lu et al. 2013). Machine settings such as transmitted ultrasound frequency, pulse repetition frequency, Doppler gain, and focal depth have been shown to influence the twinkling artifact (Aytaç and Özcan 1999; Gao et al. 2012; Kamaya et al. 2003; Tanabe et al. 2014), but also affect interaction of the acoustic wave with the stone. Rahmouni et al. (1996) initially attributed twinkling to random scattering of the ultrasound signal off rough stone surfaces. Later studies also investigated surface roughness and found that rougher stones showed more twinkling (Alan et al. 2011; Chelfouh et al. 1998; Kamaya et al. 2003; Shang et al. 2017; Wang et al. 2011; Williams et al. 2003). More recent experiments exposing *ex vivo* stones to hyper- and hypo- baric conditions found twinkling was reduced or increased, respectively, which led to the suggestion that twinkling may arise from scattering off microbubbles stabilized in crevices on the stone surface (Lu et al. 2013; Simon et al. 2018). Hyperbaric studies performed on humans provided the first evidence of these bubbles appearing on *in vivo* stones (Simon et al. 2020*)*. However, there remained some skepticism of the microbubble theory of twinkling since bubbles had not been directly observed on stones (Tanabe et al. 2014).

To observe bubbles on the stone surface, Simon et al. (2018) used long, negative pulses generated by a lithotripter to enlarge the bubbles for visualization with high-speed photography. They found that on stones that twinkled, bubbles consistently arose from the same location on the stone surface. Other researchers have evaluated kidney stone surfaces using scanning electron microscopy (SEM) and showed crevices on the stone surface where bubbles could form (Sandersius and Rez 2007); however, these scans were performed in air and thus did not allow for direct observations of bubbles. Simon et al. (2018) also proposed that

internal microbubbles may contribute to twinkling, noting voids within the stone observed with micro-computed tomography (μCT) that could harbor microbubbles (Kim et al. 2005; Williams et al. 2010; Zarse et al. 2004). Since these scans were performed on dry stones, it was impossible to determine whether low x-ray attenuation regions contained liquid or gas.

The goal of this paper is to relate surface and internal stone characteristics to microbubbles and twinkling. Thirteen *ex vivo* human kidney stones were scanned at three different frequencies to compile 3D maps of twinkling. On a subset of these stones representing a range of twinkling and surface roughness, environmental scanning electron microscopy (ESEM) and underwater μCT in ambient and hypobaric conditions were used to compare the location of bubbles to the 3D maps of twinkling.

Methods

Thirteen *ex vivo* human kidney stones were acquired from the University of Washington and Penn State Health Milton S. Hershey medical centers that ranged in composition, size, and surface roughness (Table 1). The primary composition of each stone was determined using previously established Fourier-transform infrared spectroscopy (FTIR), SEM, and/or μCT methods (Ma et al. 2018; Williams et al., 2010) and separated into calcium oxalate monohydrate (COM), calcium oxalate dihydrate (COD), uric acid (UA), ammonium urate (AU), cystine, and struvite. Stone volume was calculated by measuring the diameter in 3 dimensions with calipers and approximating the stone as an ellipsoid. Using a distinction similar to Kim et al. (2015), surface roughness was qualitatively categorized as jagged (uneven surface, many sharp points), rough (uneven, coarse surface), or smooth (uniform surface, no visible bumps). Kidney stones were submerged in deionized water for at least 1 week prior to the experiments

and degassed for >2 hours in a desiccant chamber at ~0.01 MPa absolute pressure. The exception was uric acid stones which were submerged in water and degassed for only 1 hour before imaging to prevent dissolution.

Evaluation of the twinkling artifact in 3D

Ultrasound measurements were conducted in filtered (<5 μm) and deionized water that was degassed (<2 mg/L or 20%; Extech D0210 Dissolved Oxygen Meter, Extech, Waltham, MA, USA) with a custom-built flow-through system with a gas contactor membrane (PDMSXA-2.1, PermSelect©, Ann Arbor, Michigan, USA). Ultrasound waveforms were measured in bulk water using a golden capsule hydrophone (HGL-Series, Onda, Sunnyvale, CA, USA). Three-dimensional maps of the measured Doppler power were created for each kidney stone using a research ultrasound system (Vantage, Verasonics®, Kirkland, WA, USA) with the C5-2 (Philips/ATL, Bothell, WA, USA, elevation focus = 40 mm) (2.5 MHz operating frequency, $p_+ \approx 1.37$ MPa, $p_- \approx 1.14$ MPa (in water)), L7-4 (Philips/ATL, Bothell, WA, USA) (5 MHz operating frequency, $p_+ \approx 1.68$ MPa, $p_- \approx 1.48$ MPa (in water), elevation focus = 30 mm), and L22-14v (Verasonics®, Kirkland, WA, USA) (18.5 MHz operating frequency, $p_+ \approx 1.69$ MPa, $p_- \approx 1.23$ MPa (in water), elevation focus = 10 mm) transducers. Scans were conducted using 128 elements with all three transducers. Ultrasound parameters were held constant for each transducer with 14 Doppler ensembles consisting of 7 cycles each repeated at 3000 Hz.

Each of the 13 kidney stones were placed on a 15x15x5 cm block of neoprene with the transducer placed above the stone aligned at its natural focus (Fig. 1). The transducer was mechanically scanned across the stone with the step size based on the measured -6 dB azimuthal angle for each transducer of 12.9°, 1.7°, and 0.7° for the C5-2, L7-4, and L22-14v

transducers, respectively. This resulted in step sizes of 0.5 mm for the C5-2 and L7-4 transducers, and 0.2 mm for the L22-14v transducer. The transducer was operated at a voltage just below where the splay artifact, or saturation of the received signal, occurred for each stone. While this optimized the twinkling artifact, it did result in slight differences in peak pressures between transducers and stones. In-phase quadrature (IQ) data, or demodulated radio-frequency (RF) data, was saved at approximately 1 frame per second with 2 frames averaged for each position. Each averaged slice was then compiled to create 3D representations of the Doppler signal on the stone with linear interpolation used between slices. To create accurate representations of the twinkling viewed in the real-time image, high pass filters were applied with cutoffs at 7% for L22-14v and L7-4 transducers and 2% for the C5-2 transducer. Scans were repeated three separate times with the stones positioned in the same orientation. Twinkling volumes were determined by measuring the volume of points above a threshold of 40% of the maximum Doppler power. Any signal below this threshold was translucent in the 3D map to allow for a clearer view of the higher Doppler signals which represents twinkling. To reduce the effect of stone size and allow for evaluation of stone features that contribute to twinkling, the twinkling volume was divided by the stone volume to give the percentage of the stone that twinkled.

Statistical analysis

Statistical analyses were performed using Microsoft Excel (Excel, Microsoft, Redmond, Washington) along with the Real Statistics Resource Pack software by Charles Zaiontz. Values reported for each stone and frequency are the mean value over the three scans and uncertainties are given as ±1 standard deviation. To compare the effect of frequency on the

percentage of the stone volume that twinkled, the median and interquartile range (IQR) of all thirteen stones at each frequency was calculated. A non-parametric Friedman test ($\alpha<0.05$) was conducted with post hoc comparisons performed using a Nemenyi test to determine statistical significance (Friedman 1937; Demšar 2006).

Evaluation of stone characteristics

Three stones (7, 2, and 8) were selected for scanning electron microscopy and chosen to represent a range of surface roughness. Each stone was imaged with an environmental scanning electron microscope (ESEM; FEI XL-20, Philips, Amsterdam, Netherlands) at 20 kV with temperature and pressure varied to increase the relative humidity from 90% at ~0.5% intervals every 2 minutes. The size of crevices where water first condensed were tracked and compared to the general twinkling characteristics of the stone at 5 MHz.

Three stones (10, 11, and 5) displaying a range of twinkling were scanned with micro-computed tomography (µCT; 6 µm isotropic resolution; 300 kV v|tome|x L300, GE, Boston, NY USA) while submerged in deionized and degassed water to evaluate internal features that may contribute to twinkling. Stones were consecutively scanned in ambient and hypobaric conditions of ~0.02 MPa absolute to evaluate for gas within low x-ray attenuation regions. All µCT data were analyzed with ImageJ (NIH, Bethesda, MD, USA) and gas volumes were extracted using Avizo® (ThermoFisher Scientific, Waltham, MA, USA). A non-local means filter was applied to reduce noise and the scan was segmented into 'stone', 'water', and 'gas' based on thresholds set by the density of the water surrounding the stone. Box plots showing the distribution of individual gas volumes were created for stones with gas present in ambient and hypobaric conditions.

Results

Sizing and locating twinkling

Three-dimensional maps of twinkling were created for all thirteen stones (Fig. 2) and used to calculate the percentage of the stone volume that twinkled (Fig. 3) for each of the three tested frequencies. Scans repeated over three days showed relatively consistent volumes of twinkling with maximum standard deviations of 1.19%, 0.83%, and 0.36% for 2.5, 5, and 18.5 MHz, respectively, which were observed to arise from the same locations. The median and IQR of the percentage of the stone volume that twinkled for all 13 stones scanned at 2.5, 5, and 18.5 MHz are 0.40% (IQR = 0.20-1.7%), 0.56% (IQR = 0.066-2.0%), and 0.032% (IQR = 0.0029-0.10%), respectively. There was a statistically significant difference in the percentage of the stone volume that twinkled across the three tested frequencies ($\chi_F^2(2)$ = 15.64, p < 0.001). Post hoc comparisons indicated there was no significant difference (p = 0.95) between the percentage of the stone volume that twinkled at 2.5 and 5 MHz. However, the percentage of the stone volume that twinkled at 2.5 and 5 MHz was significantly greater than the percentage of the stone volume that twinkled at 18.5 MHz (p = 0.014 and p = 0.022, respectively). Between stones, there was significant variation of the size of the twinkling artifact with 3/3 jagged, 1/5 rough, and 1/5 smooth stones twinkling across >1% of the total stone volume at 2.5 and/or 5 MHz. Similarly, categorizing stones by composition showed 1/3 COM, 1/2 COD, 0/2 UA, 2/2 AU, 1/2 cystine, and 0/2 struvite stones twinkled across >1% of the total volume at 2.5 and/or 5 MHz.

Evaluation of stone characteristics

ESEM scans of stones 7, 2, and 8 showed locations of surface pores where water first condensed for comparison to the twinkling artifact. Stone 7 (smooth, COD) had the smallest percentage of stone twinkling at 0.56% and a surface comprised of small, shallow crevices 1-25 μm diameter (Fig. 4B). Stone 2 (rough, struvite), for which 0.83% of the stone twinkled, showed many crevices that were relatively deep and 1-25 μm in diameter (Fig. 4G). Stone 8 (jagged, COD) had the most twinkling at 2.0% of the stone volume and was comprised of both deep and shallow crevices 1-10 μm diameter (Fig. 4L). In all three stones, water began to condense in the smallest visible crevices of ~1 μm in diameter, but condensation occurred at different relative humidities of 95% for stone 2 (Fig. 4H-J) compared to 100% for stones 7 (Fig. 4C-E) and 8 (Fig. 4M-O). In stone 2, condensation subsequently occurred in larger crevices as the relative humidity continued to increase.

When the kidney stones were imaged while submerged in water with μCT at ambient pressure, low-density cracks and crevices were observed at discrete locations throughout all stones (Fig. 5B,G,L). When stones were subsequently imaged in hypobaric conditions, the size of the low-density volumes increased in stones 11 (Fig. 5C) and 10 (Fig. 5H) but did not change in stone 5 (Fig. 5M). Stone 11, which had the least twinkling over its volume at 0.059%, contained voids near the center that expanded from 0.14 mm^3 to 0.15 mm^3, an increase of ~7% (Fig. 5D-E). Stone 10, for which 0.22% of the stone twinkled, contained low-density voids in cracks throughout the stone that expanded from 4.9 x 10^{-3} mm^3 to 250 x 10^{-3} mm^3, an increase of ~5000% (Fig. 5I-J). In stone 5 with the highest twinkling at 2.4%, low-density voids filled with water were present throughout the entire stone and did not change when the pressure was reduced (Fig. 5N-O).

Figure 6 shows the distribution of individual 'gas' volumes for stones 10 and 11 in ambient and hypobaric conditions. In ambient conditions, stone 10 had 194 discrete gas volumes with an average volume of 0.0063 x 10^{-3} mm^3 while stone 11 had 65 discrete gas volumes with an average volume of 2.2 x 10^{-3} mm^3. In hypobaric conditions, the number of discrete gas volumes in stone 10 decreased to 51 and the average bubble size increased to 4.9 x 10^{-3} mm^3. Comparatively, in stone 11 the number of discrete gas volumes increased to 80 but the average volume decreased slightly to 1.9 x 10^{-3} mm^3. Thus, both stones showed an overall increase in total gas volume in hypobaric conditions – in stone 10 through fewer, larger gas pockets and in stone 11 through more, smaller gas pockets.

Discussion

These results support the microbubble theory of twinkling and provide evidence that bubbles could be external as well as internal to the stone. Ultrasound scans performed on thirteen kidney stones at three different frequencies showed a larger volume of the stone twinkled at 2.5 and 5 MHz compared to 18.5 MHz, which is consistent with previous work (Gao et al. 2012). In addition, twinkling was observed to arise from the same location on each stone with repeated imaging suggesting that physical features at specific locations on the stone cause the twinkling artifact. Care must be taken when interpreting these results due to inherent effects of different frequencies. As frequency increases, the wavelength decreases, thus increasing the resolution of the 3D maps, absorption from the stone, and scattering from the rough surface and microbubbles. These effects can be noted in Fig. 2 where the 3D map at 2.5 MHz produced a less defined image of the stone than at 18.5 MHz. Additionally, though effort was taken to compare frequencies with similar pressures, there are significant differences in

resolution and sensitivity between transducers that are not considered here. Future work includes scanning stones with multiple frequencies from a single transducer.

Interestingly, the percentage of the stone that twinkled did not track with expectations of twinkling based on macroscopic surface roughness in that some smooth stones twinkled more than some jagged or rough stones. This may be explained through the ESEM scans as microscopic crevices of similar diameters, but different surface densities, were observed for all three macroscopic surface types. Due to constraints in the experimental configuration, the exact scanning location on the stone with ESEM is unknown, making it impossible to correlate stone surface features with exact twinkling locations or features from the μCT images. Additionally, gas pockets internal to the stone may also contribute to differences in twinkling. In 2/3 smooth stones scanned with μCT, low-density volumes expanded when the ambient pressure was reduced indicating the presence of internal microbubbles. While both stones with internal microbubbles twinkled, the stone with the largest percentage of twinkling (stone 5) did not contain any internal microbubbles. Thus, these results suggest many factors internal and external to the stone contribute to the location and size of the twinkling artifact.

In ESEM scans of all three macroscopic surface roughness, water condensed first in the smallest resolvable crevices (~1 μm in diameter), which could indicate those crevices are more likely to harbor bubbles. It is well known that small surface defects can enable consistent bubble nucleation (Liger-Belair at al. 2008). Although urine is not supersaturated with gas (typically containing ~4 mg/L, 40% oxygen saturation (Giannakopoulos, et al. 1997)), it is possible for bubbles to form in crevices even in fluids with little gas concentration (Ryan and Hemmingsen 1998). Neglecting the boundary effects of the crevices, if bubbles formed in the

smallest pores (~1 μm), the Minnaert resonance frequency of the bubbles would be ~3.29 MHz (Minnaert 1933). This may explain why twinkling comprised more of the stone volume at 2.5 MHz and 5 MHz compared to 18.5 MHz.

The μCT scans of stones at ambient and hypobaric conditions provided the first evidence of gas inside some kidney stones. Low-density voids in stone 10 were found to expand in cracks throughout the stone when the pressure was reduced. Conversely, in stone 11 the low-density voids were concentrated near the stone center with very little room to expand. These observations could explain why twinkling covered more of the surface on stone 10 (Fig. 5F) compared to the small localized area of twinkling on stone 11 (Fig. 5A). The stone that twinkled the most (stone 5) did not contain any internal microbubbles, suggesting other factors contributed to its twinkling. It is important to note that stones 5 and 11 were both primarily cystine, but showed significantly different internal microarchitectures and twinkling characteristics. The μCT scans were performed with the stone in the same configuration as was used for ultrasound scanning, thus, the ultrasound maps and μCT volume renderings in Fig. 5 can be compared directly. However, we are unable to distinguish between the effects of internal and external features on twinkling.

The primary limitation to this study was the use of *ex vivo* kidney stones that were completely dried out before being rehydrated and degassed for the scans. It is possible that gas observed inside the stones was artificially introduced into the stone and would not be present in *in situ* kidney stones. In addition, only thirteen stones were scanned with ultrasound and an even smaller subsets of stones were scanned with μCT and ESEM. Significant variability exists between individual kidney stones that was not captured when categorizing stones by size,

macroscopic roughness, composition, or twinkling, prompting the need for additional studies with many fresh kidney stones to support these results. Other future work includes growing and imaging pure crystals to observe the isolated effect of chemical composition on twinkling as well as additional human studies in hyperbaric/hypobaric conditions prior to stone removal for analysis. Both studies would provide further evidence that bubbles are present on *in vivo* kidney stones.

Conclusion

These studies show internal and external bubbles may exist on kidney stones and contribute to the twinkling artifact. Stones imaged with three different frequencies showed twinkling was consistent and covered more of the stone volume at lower frequencies. ESEM scans showed microscopic crevices on all macroscopic stone surface types and that water first condensed in the smallest (~1 μm diameter) crevices on the stone surface. Additionally, kidney stones imaged underwater with μCT showed bubbles were present inside some stones as the volume of gas increased when the ambient hydrostatic pressure was reduced. These results provide additional insight into the origins of the twinkling artifact and may aid in improving ultrasound-based kidney stone diagnoses and treatments.

Acknowledgements

The authors would like to thank Timothy Stecko of the Pennsylvania State University Energy and Environmental Sustainability Laboratories for help in designing and implementing the hypobaric μCT scanning. This material is based in part upon work supported by the National Science Foundation under Grant No. 1943937.

References

Alan C, Koçoglu H, Kosar S, Karatag O, Resit Ersay A, Erhan A. Role of twinkling artifact in characterization of urinary calculi. Actas Urol Esp 2011;35:396-402.

Aytaç SK, Ozcan H. Effect of color Doppler system on the twinkling sign associated with urinary tract calculi. J Clin Ultrasound 1999;27(8):433-439.

Chelfouh N, Grenier N, Higueret D, Trillaud H, Levantal O, Pariente J, Ballanger P. Characterization of urinary calculi: In vitro study of "twinkling artifact" revealed by color-flow sonography. Am J Roentgenol 1998;171:1055-1060.

Demšar J. Statistical comparisons of classifiers over multiple data sets. J Mach Learn Res 2006;7:1-30.

Dillman JR, Kappil M, Weadock WJ, Rubin JM, Platt JF, DiPietro MA, Bude RO. Sonographic twinkling artifact for renal calculus detection: correlation with CT. Radiology 2011;259(3):911-916.

Friedman, M. The use of ranks to avoid the assumption of normality implicit in the analysis of variance. J Am Stat Assoc 1937;32(200):675-701.

Gao J, Hentel K, Rubin JM. Correlation between twinkling artifact and color Doppler carrier frequency: preliminary observations in renal calculi. Ultrasound Med Biol 2012;38(9):1534-1539.

Giannakopoulos X, Evangelou A, Kalfakakou V, Grammeniatis E, Papandropoulos I, Charalambopoulos K. Human bladder urine oxygen content: implications for urinary tract diseases 1997;29(4):393-401.

Kamaya A, Tuthill T, Rubin, JM. Twinkling artifact on color Doppler sonography: Dependence on machine parameters and underlying cause. Am J Roentgenol 2003;180:215-222.

Khan SR, Pearle MS, Robertson WG, Gambaro G, Canales BK, Doizi S, Traxer O, Tiselius H. Kidney stones. Nat Rev Dis Primers 2016;2:16008.

Kielar AZ, Shabana W, Vakili M, Rubin JM. Prospective Evaluation of Doppler Sonography to Detect the twinkling artifact versus unenhanced computed tomography for identifying urinary tract calculi. J Ultrasound Med 2012;31:1619-1625.

Kim SC, Hatt EK, Lingeman JE, Nadler RB, McAteer JA, Williams JC. Cystine: Helical computerized tomography characterization of rough and smooth calculi in vitro. J Urol 2005;174:1468-1471.

Korkmaz M, Aras B, Şanal B, Yücel M, Güneyli S, Koçak A, Uruç F. Investigating the clinical significance of twinkling artifacts in patients with urolithiasis smaller than 5 mm. Jpn J Radiol 2014;32:482-486.

Lee JY, Kim SH, Cho JY, Han D. Color and power Doppler twinkling artifacts from urinary stones: clinical observations and phantom studies. Am J Roentgenol 2001;176:1441-1445.

Liger-Belair G, Polidori G, Jeandet P. Recent advances in the science of champagne bubbles. Chem Soc Rev 2008;37(11):2490-2511.

Lu W, Sapozhnikov OA, Bailey MR, Kaczkowski PJ, Crum LA. Evidence for Trapped Surface Bubbles as the cause for the twinkling artifact in ultrasound imaging. Ultrasound Med Biol 2013:39(6):1026-1038.

Ma R, Luo X, Li Q, Zhong H.The systematic classification of urinary stones combine-using FTIR and SEM-EDAX. Int J Surg 2017;41:150-161.

Masch WR, Cohan RH, Ellis JH, Dillman JR, Rubin JM, Davenport MS. Clinical effectiveness of prospectively reported sonographic twinkling artifact for the diagnosis of renal calculus in patients without known urolithiasis. Am J Roentgenol 2016;206:326-331.

Minnaert M. On musical air bubbles and the sounds of running water. Philos Mag 1933;16;235-248.

Mitterberger M, Aigner F, Pallwein L, Pinggera G, Neururer R, Rehder P, Frauscher F. Sonographic detection of renal and ureteral Stones. International Braz J Urol 2009;35(5):532-541.

Park SJ, Yi BH, Lee HK, Kim YH, Kim GJ, Kim HC. Evaluation of patients with suspected ureteral calculi using sonography as an initial diagnostic tool: how can we improve diagnostic accuracy? J Ultrasound Med 2008;7:1441-1450.

Rahmouni A, Bargoin R, Herment A, Bargoin N, Vasile N. Color Doppler twinkling artifact in hyperechoic regions. Radiology 1996;199(1):269-271.

Ryan WL, Hemmingsen, EA. Bubble formation at porous hydrophobic surfaces. J Colloid Interface Sci 1998;197:101-107.

Sandersius S, Rez P. Morphology of crystals in calcium oxalate monohydrate kidney stones. Urol Res 2007;35:287-293.

Shabana W, Bude RO, Rubin JM. Comparison between color Doppler twinkling artifact and acoustic shadowing for renal calculus detection: an in vitro study. Ultrasound Med Biol 2009;35(2):339-350.

Shang M, Sun X, Liu Q, Li J, Shi D, Ning S, Cheng L. Quantitative evaluation of the effects of urinary stone composition and size on color doppler twinkling artifact: A phantom study. J Ultrasound Med 2017;36:733-740.

Simon JC, Sapozhnikov OA, Kreider W, Breshock M, Williams JC, Bailey MR. The role of trapped bubbles in kidney stone detection with the color Doppler ultrasound twinkling artifact. Phys Med Biol 2018;63(2):025011.

Simon JC, Holm JR, Thiel J, Dunmire B, Cunitz BW, Bailey MR. Evidence of microbubbles on kidney stones in humans. Ultrasound Med Biol 2020;46(7):1802-1807.

Smith RC, Varanelli M. Diagnosis and management of acute ureterolithiasis: CT is truth. Am J Roentgenol 2000;175:3-6.

Sorensen MD, Harper JD, Hsi RS, Shah AR, Dighe MK, Carter SJ, Moshiri M, Paun M, Lu W, Bailey M. B-mode ultrasound versus color doppler twinkling artifact in detecting kidney stones. J Endourol 2003;27(2):149-153.

Tanabe M, Naito Y, Nishimot M, Liu L. Effect of pulse repetition frequency on microcalcification detection in color flow imaging. Jpn J Appl Phys 2014;53:07KF15.

Trillaud H, Pariente J, Rabie A, Grenier N. Detection of encrusted indwelling ureteral stents using a twinkling artifact revealed on color Doppler sonography. Am J Roentgenol 2001;176:1447-1448.

Turrin A, Minola P, Costa F, Cerati L, Andrulli S, Trinchieri A. Diagnostic value of colour Doppler twinkling artefact in sites negative for stones on B mode renal sonography. Urol Res 2007;35:313-317.

Wang M, Li J, Xiao J, Shi D, Zhang K. Systematic analysis of factors related to display of the twinkling artifact by a phantom: an optimized investigation. J Ultrasound Med 2011;30:1449-1457.

Williams JC, McAteer JA, Evan AP, Lingeman JE. Micro-computed tomography for analysis of urinary calculi. Urol Res 2010;38:477-484.

Williams JC, Saw KC, Paterson RF, Hatt EK, McAteer JA, Lingeman JE. Variability of renal stone fragility in shock wave lithotripsy. Urology 2003;61(6):1092-1097.

Winkel RR, Kalhauge A, Fredfeldt K. The usefulness of ultrasound colour-Doppler twinkling artefact for detecting urolithiasis compared with low dose nonenhanced computerized tomography. Ultrasound Med Biol 2012;38(7):1180-1187.

Wood G, Urban MW. Detecting kidney stones using twinkling artifacts: Survey of kidney stones with varying composition and size. Ultrasound Med Biol 2020;46:156-166.

Zarse CA, McAteer JA, Sommer AJ, Kim SC, Hatt EK, Lingeman JE, Evan EP, Williams JC. Nondestructive analysis of urinary calculi using micro computed tomography. BMC Urology 2004;4:15.

Figure Captions

Fig. 1. Diagram of the experimental arrangement for 3D ultrasound scans of the kidney stones.

Fig. 2. Representative 3D maps of the Doppler signal measured on stones 8 *(upper)* and 5 *(lower)* at 2.5, 5, and 18.5 MHz. Scanning was performed in the azimuthal direction, indicated by the dashed arrow. Twinkling was observed on stone 8 over 0.49%, 2.0%, and 0.032% of the stone volume at 2.5, 5, and 18.5 MHz, respectively. Comparatively on stone 5 twinkling was observed over 1.9%, 2.4%, and 0.094% of the stone volume at 2.5, 5, and 18.5 MHz, respectively.

Fig. 3. Graph showing percentage of the stone volume that twinkled versus each of the 13 stones for the 3 tested frequencies. Error bars represent the standard deviation between trials.

Fig. 4. Column 1: 3D representations of twinkling on stones 7, 2, and 8. Twinkling was found over (A) 0.56%, (F) 0.83%, and (K) 2.0% of the stone volumes, respectively. Columns 2-5: Environmental scanning electron microscope (ESEM) images of each kidney stone at 93% relative humidity and as the relative humidity increased over time. Red dashed boxes (B,G,L) indicate the regions of interest magnified in the subsequent images. In all stones, water first condensed in the smallest visible crevices (~1 μm, red circles). For stones 7 and 8, water began condensing at 100% relative humidity (C-E,M-O), while for stone 2, water began condensing at 95% relative humidity (H-J).

Fig. 5. Column 1: 3D representations of twinkling on stones 11, 10, and 5. Twinkling was found over (A) 0.02%, (F) 0.2%, and (K) 2.4% of the stone volumes. Columns 2+3: Same slices of each kidney stone scanned with micro-computed tomography (μCT) in ambient and hypobaric conditions. (B-C) In stone 11, low density voids are present near the center of the stone and

only expanded slightly (dotted yellow ovals) when pressure decreased. (G-H) In stone 10, low density voids expanded significantly (dashed yellow ovals) when pressure decreased. (L-M) In stone 5, low density voids are present throughout the stone, but did not expand when pressure decreased. Columns 4+5: Volume rendering of stone scanned with µCT in ambient and hypobaric conditions with low-density volumes segmented out in blue. The low-density volume increased with decreased pressure in (D-E) stone 11 (7%) and (I-J) stone 10 (3000%) while (N-O) not changing in stone 5.

Fig. 6. A box plot representing the volume of individual low-density, or gas, volumes from µCT scans of stones 10 and 11 in ambient and hypobaric pressures. In both stones, the total volume of gas increased upon reducing the ambient pressure, but the mean bubble size increased in stone 10 while decreasing in stone 11. Gas volumes sized larger than 0.01 mm^3 are excluded from the graph for clarity.

Tables

Table 1. Kidney stones listed in order of ascending volume with surface and chemical type.

Stone	Volume (mm^3)	Surface Type	Chemical Type	Picture
1	4.1	Jagged	AU	
2	33.5	Rough	Struvite	
3	35.3	Jagged	COM	
4	39.3	Rough	AU	
5	60.0	Smooth	Cystine	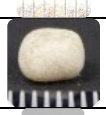
6	66.2	Rough	COD	
7	71.0	Smooth	COM	
8	89.1	Jagged	COD	
9	128.0	Rough	UA	
10	207.6	Smooth	Struvite	
11	221.8	Smooth	Cystine	
12	282.6	Rough	UA	
13	547.9	Rough	COM	

Figures

Fig. 1. Diagram of the experimental arrangement for 3D ultrasound scans of the kidney stones.

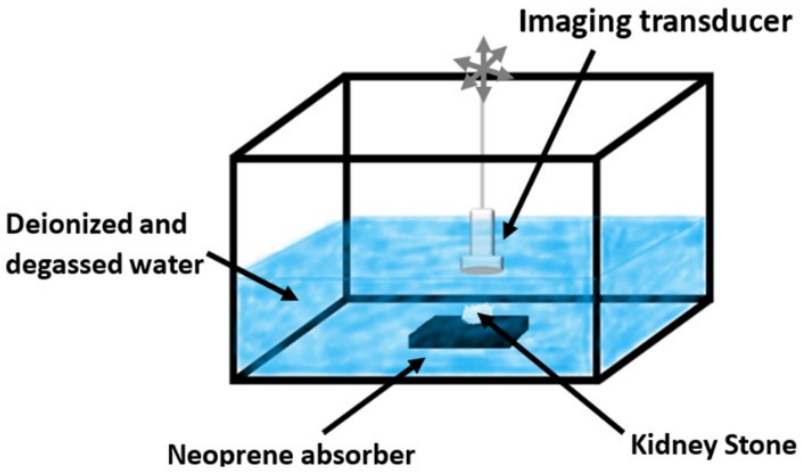

Fig. 2. Representative 3D maps of the Doppler signal measured on stones 8 *(upper)* and 5 *(lower)* at 2.5, 5, and 18.5 MHz. Scanning was performed in the azimuthal direction, indicated by the dashed arrow. Twinkling was observed on stone 8 over 0.49%, 2.0%, and 0.032% of the stone volume at 2.5, 5, and 18.5 MHz, respectively. Comparatively on stone 5 twinkling was observed over 1.9%, 2.4%, 0.094% of the stone volume at 2.5, 5, and 18.5 MHz, respectively.

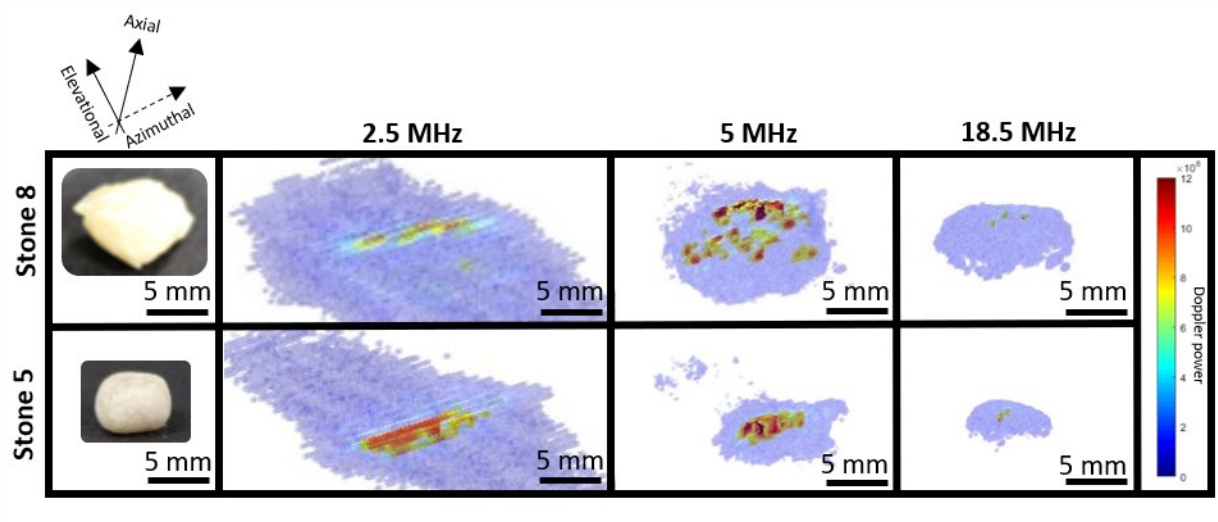

Fig. 3. Graph showing percent of the stone volume that twinkled versus each of the 13 stones for the 3 tested frequencies. Error bars represent the standard deviation between trials.

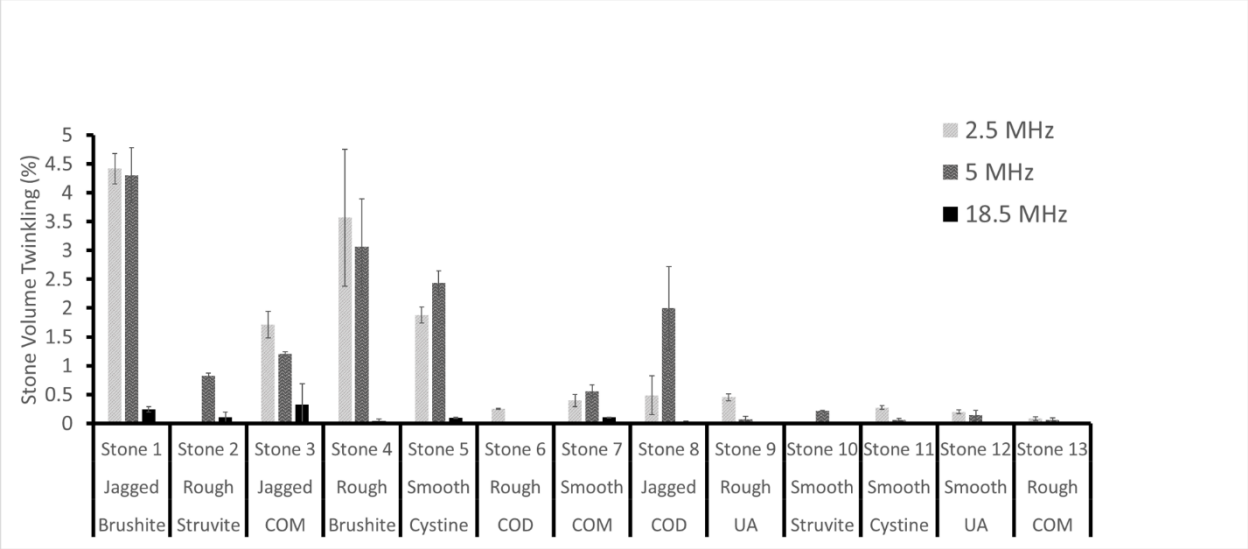

Fig. 4. Column 1: 3D representations of twinkling on stones 7, 2, and 8. Twinkling was found over (A) 0.56%, (F) 0.83%, and (K) 2.0% of the stone volumes, respectively. Columns 2-5: Environmental scanning electron microscope (ESEM) images of each kidney stone at 93% relative humidity and as the relative humidity increased over time. Red dashed boxes (B,G,L) indicate regions of interest in the subsequent measurements. In all stones, water first condensed in the smallest visible crevices (~1 µm, red circles). For stones 7 and 8, water began condensing at 100% relative humidity (C-E,M-O), while for stone 2, water began condensing at 95% relative humidity (H-J).

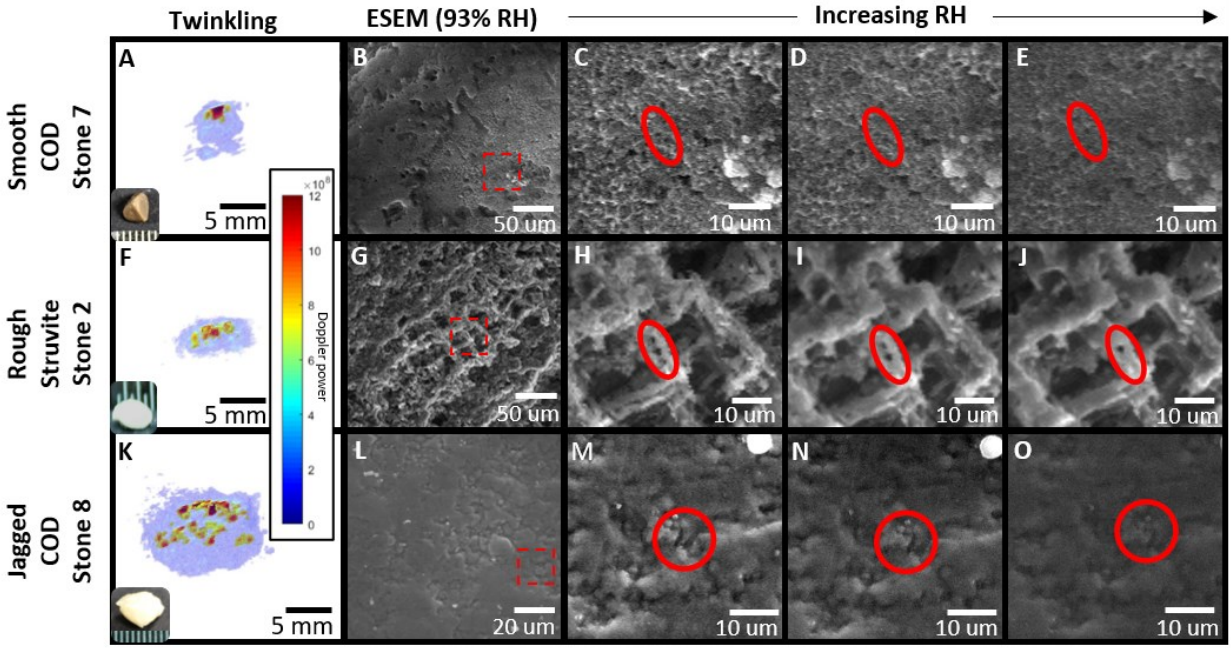

Fig. 5. Column 1: 3D representations of twinkling on stones 11, 10, and 5. Twinkling was found over (A) 0.02%, (F) 0.2%, and (K) 2.4% of the stone volumes. Columns 2+3: Same slices of each kidney stone scanned in ambient and hypobaric conditions. (B-C) In stone 11, low density voids are present near the center of the stone and only expanded slightly (yellow circles) when pressure decreased. (G-H) In stone 10, low density voids expanded significantly (red circles) when pressure decreased. (L-M) In stone 5, low density voids are present throughout the stone, but did not expand when pressure decreased. Columns 4+5: Volume rendering of stone scanned with µCT in ambient and hypobaric conditions with low-density volumes segmented out in blue. The low-density volume increased with decreased pressure in (D-E) stone 11 by 7% and (I-J) stone 10 by 3000% while not changing in (N-O) stone 5.

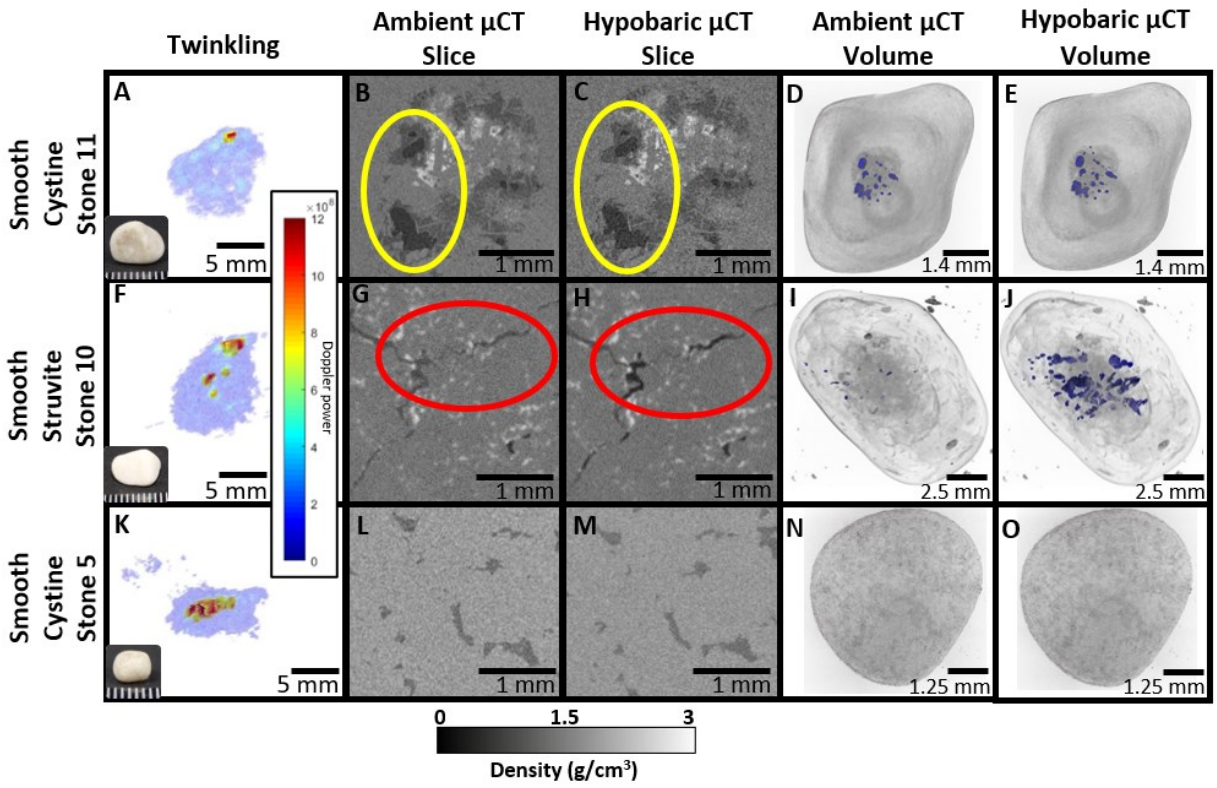

Fig. 6 - A box plot representing the volume of individual low-density, or gas, volumes from µCT scans of stones 10 and 11 in ambient and hypobaric pressures. In both stones, the total volume of gas increased upon reducing the ambient pressure; however the mean bubble size increased in stone 10 while decreasing slightly in stone 11. Gas volumes sized larger than 0.01 mm^3 are excluded from the graph for clarity.